Materials Science & Engineering A 771 (2020) 138650

Contents lists available at ScienceDirect

Materials Science & Engineering A

journal homepage: http://www.elsevier.com/locate/msea

Stimulated heterogeneous distribution of Sc element and its correlated local hardening effect in Al–Fe–Ni-Sc alloy

Zeyu Bian [a,b], Yakai Xiao [a,b], Lei Hu [a], Yingtao Liu [a], Zhe Chen [a], Mingliang Wang [a,*], Dong Chen [b,c,**], Haowei Wang [a,b]

[a] School of Materials Science & Engineering, Shanghai Jiao Tong University, Shanghai, 200240, China
[b] State Key Laboratory of Metal Matrix Composites, Shanghai Jiao Tong University, Shanghai, 200240, China
[c] Anhui Aluminium Matrix Composites Engineering Research Centre, Huaibei, China

ARTICLE INFO

Keywords:
Stimulated heterogeneous distribution
Aluminum alloys
Sc element
Hardness
Precipitation
Casting

ABSTRACT

This work studied the stimulated heterogeneous distribution behavior of Sc element and the correlated local hardening effect in the eutectic Al–Fe–Ni alloy. Through microstructure characterizations, Sc was found to aggregate along grain boundaries, namely eutectic phase free areas. The aggregation behavior made the Sc concentration in eutectic phase free areas reach even twice of nominal addition, which was more uneven than Sc in Al–Sc alloy. Meanwhile, tiny Al grains were induced in eutectic phase free areas when the Sc addition exceeded 0.3 wt%. These stimulated heterogeneous distribution behaviors were attributed to solute redistribution exacerbated by the eutectic structure, and discussed by a modified Scheil Equation analytically. Furthermore, nanoindentation tests demonstrated a local hardening behavior correlated with the stimulated heterogeneous distribution of Sc element. Through a quantitatively explanation, it was finally concluded that the inhomogeneous distribution of Sc element can effectively induce the strengthening effect to the eutectic alloy at macro scale.

1. Introduction

Sc-containing Al alloys have received intensive interests in recent decades [1–3]. Among these researches, the Sc distribution is a basic topic since it is the precondition to microstructural and mechanical evolutions in Al–Sc alloys. Typically, Sc is inclined to segregate at grain boundaries (GBs) in Al alloys [4,5], which is described by Scheil Equation to explain solute redistribution behavior during the solidification. Furthermore, Sc was found to micro-segregated in the interdendritic zones, and formed the harmful (Cu, Sc)-rich W-phases in Al–Cu-Sc alloy [6]. However, the research on the distribution behavior of Sc under the existence of other elements is still limited.

With the development of Al–Sc alloys, two aspects can be divided according to the functions of Sc. First, Sc is to form $L1_2$-Al_3Sc crystals in Al alloys. Al_3Sc is the efficient nuclei of α-Al to refine and stabilize Al grains [1–3,7,8]. The successful examples ascribed to this category include Al–Mg-Sc-Zr and Al–Zn–Mg-Sc-Zr alloys [8–11]. Second, Sc is used to induce strengthening effect on Al alloys at both room and high temperature (HT) by precipitation strengthening. Al_3Sc precipitates are capable of strengthening Al significantly, arising from anti-phase boundary energy, coherency stain and modulus mismatch [12,13]. Meanwhile, Al_3Sc precipitates can keep stable above 300 °C for a long time without coarsening because of the low diffusion rate of Sc in Al matrix [13–15]. For instance, Gao et al. [16–18] reported that the heat resistance and creep performance of Al–Cu alloys were effectively promoted by Al_3Sc precipitates.

However, the high diffusion rate of Cu limits the further revision of these Al alloys at HT [19]. Novel eutectic alloys (i.e., Al–Fe, Al–Ni, Al–Fe–Ni and Al–Fe-RE alloys) have been extensively studied due to their lower diffusion rates and phase stabilities at HT [20–24]. Adding Sc to these eutectic systems can further improve HT performance of Al alloys. For example, Suwanpreecha et al. [21] reported that Al–Ni-Sc alloy possessed superior tensile performance and stability at HT. Furthermore, they demonstrated that adding Sc can effectively improve the creep performance of the eutectic Al–Ni at 300 °C [25]. Similarly, the development of eutectic alloys like Al–Ni–Zr and Al–Ni–Zr–Si–Er

* Corresponding author.
** Corresponding author. State Key Laboratory of Metal Matrix Composites, Shanghai Jiao Tong University, Shanghai, 200240, China.
E-mail addresses: mingliang_wang@sjtu.edu.cn (M. Wang), chend@sjtu.edu.cn (D. Chen).

https://doi.org/10.1016/j.msea.2019.138650
Received 14 October 2019; Received in revised form 5 November 2019; Accepted 6 November 2019
Available online 7 November 2019
0921-5093/

declared the improved tensile strength, coarsening and creep resistance compared to Al–Ni or Al–Zr matrix alloys at high temperatures [26,27]. Although the improvement on mechanical performance has been confirmed, there is rarely report on element distribution behavior in the eutectic alloy, and the influence of this behavior on mechanical performance. Since the eutectic alloys have the different solidification behavior from pure Al, the distribution of element like Sc should be deeply affected, and thereby the strengthening performance to eutectic alloys.

As a typical eutectic alloy, the Al–Fe–Ni alloy has potential applications in the electronic and electric fields owing to the lower solubility of both Ni and Fe elements in Al [28]. Meanwhile, the alloy can be used as the nuclear fuel cladding material for its good corrosion resistance in liquid at high temperature [29,30]. In addition, the Al–Fe–Ni alloy owns superior high temperature performance and heat resistance over the traditional Al–Si alloy [22,31,32]. Based on these points, our work investigates the stimulated heterogeneous distribution (SHD) behavior of Sc element in eutectic Al-1.75Fe-1.25Ni alloy. The SHD phenomenon is discussed correlated with the eutectic features. Furthermore, a modified Scheil Equation is used to describe the SHD behavior analytically. Finally, the Vickers hardness and nanoindentation tests are performed and correlated with microstructure evolutions quantitatively in the Al–Fe–Ni-*x*Sc alloy.

2. Experiments

2.1. Materials preparation

The Al-1.75Fe-1.25Ni-*x*Sc ($x = 0$, 0.1, 0.2, 0.3 wt%) alloys (Brevity for Al–Fe–Ni-*x*Sc hereafter) were prepared using the conventional gravity cast, and the detailed information was provided in our former report [22]. The elemental compositions of these alloys were measured by the inductively coupled plasma-atomic emission spectrometry (ICP-AES). The nominal compositions of Al–Fe–Ni-xSc alloys are in good accordance with ICP results (Table 1), showing that these alloys have been successfully controlled in the casting. Practically, both Fe and Ni compositions are locating at Al–Al_9FeNi eutectic region of the alloy [33].

2.2. Microstructure characterization and mechanical testing

The Scanning Electron Microscope (SEM, TESCAN) and Electron Back-Scattered Diffraction (EBSD) technique were used to characterize the microstructure. Al_3Sc precipitates were analyzed by Transition Electron Microscope (TEM, JEM2100F). The macro-hardness was tested by Vickers hardness (EZ-mat, CARAT930), and the micro-hardness of local area was performed by nanoindentation (HYSITRON, TI950). To quantify the microstructure features of the alloy, we normally analyzed the SEM images with the aid of the Image J software. For example, the average eutectic sub-grains size in the alloy was measured in the SEM micrographs using the Image J software. In these micrographs, more than 50 sub-grains were chosen randomly and analyzed hereby. In detail, the average value of equivalent diameter was adopted as the average eutectic sub-grains size.

Table 1
The compositions of Al–Fe–Ni-*x*Sc alloys (wt%).

Alloy	Nominal compositions			ICP results		
	Fe	Ni	Sc	Fe	Ni	Sc
Al–Fe–Ni	1.75	1.25	–	1.67	1.25	
Al–Fe–Ni-0.1Sc	1.75	1.25	0.1	1.65	1.23	0.09
Al–Fe–Ni-0.2Sc	1.75	1.25	0.2	1.64	1.26	0.18
Al–Fe–Ni-0.3Sc	1.75	1.25	0.3	1.66	1.23	0.31

3. Results

3.1. The microstructures of Al–Fe–Ni-xSc alloys and their formation process

Fig. 1a–d shows the as-cast microstructures of Al–Fe–Ni-*x*Sc ($x = 0$, 0.1, 0.2, 0.3 wt%) alloys, accordingly. In Al–Fe–Ni alloy (Fig. 1a), the eutectic grains can be seen separated by eutectic boundary Al, which is also named as eutectic phase free area (EPFA). With the increasing Sc addition, the microstructures of Al–Fe–Ni-*x*Sc ($x = 0.1$, 0.2, 0.3 wt%) alloys present the similar morphologies with the Al–Fe–Ni alloy.

The shape and composition of eutectic phases in the Al–Fe–Ni alloys are exhibited in Fig. 1e. The eutectic phases inside the eutectic grain have the needle-like shape. These phases have the diameter from 200 to 300 nm in cross-section, and they are likely to penetrate the entire grain straightly with paralleling to each other. However, the shape of the eutectic phases alongside the GB shows a change. These phases appear to be flake-like according to the block-like surface exhibited in Fig. 1e, and rod-like section exhibited in Fig. 1a. The compositions of these phases are also shown in embedded table (Fig. 1e). Both the needle-like phase inside grain and the flake-like phase along GB are considered as Al_9FeNi.

In Al–Fe–Ni-*x*Sc alloys, the shapes of Al_9FeNi phase inside grain and alongside GB are hardly affected (Fig. 1b–d). Also, the phase compositions keep unchanged as Al_9FeNi with increasing Sc addition, as shown in XRD patterns (Fig. 1f). Overall, the microstructures of all these alloys exhibited similar features, indicating that adding Sc rarely changes the eutectic structure of Al–Fe–Ni alloy.

The Al–Fe–Ni alloy is a metal-metal type eutectic alloy, and the mass fraction of Al_9FeNi corresponding to the eutectic composition is ~12 wt %. In Al-1.75Fe-1.25Ni alloy, the mass fraction of Al_9FeNi is ~10.6 wt%, of which the volume fraction is ~8.4 vol%. The eutectic phase of a metal-metal type eutectic alloy exhibits a needle-like shape when the volume fraction of eutectic phase below 27.6% [34], while it turns to be flake-like when the volume fraction of eutectic phase over 27.6%. Therefore, the majority Al_9FeNi phases in this alloy are observed to be needle-like.

The phase shape change of Al–Fe–Ni alloy exhibited in eutectic structure is attributed to the solute redistribution during solidification. This process can be estimated quantitatively by the solidus and liquidus according to phase diagram, which is described by $k_0 = C_s/C_l$ (Here, C_s and C_l are the compositions of the solid or liquid phase in phase diagram, respectively) [35–37]. The k_0 of hypoeutectic composition is basically recognized to be less than 1 [34], indicating that the solute atoms tend to be pushed from solid and gathered at the melt. As the process of solidification continues, more and more solute atoms aggregates in the melt, causing that the volume fraction of eutectic phase composition surpasses 27.6%. Therefore, the shape of Al_9FeNi changes to be flake-like at the end of solidification, which is corresponding to the phase observed near the GB (Fig. 1e). Due to the consumption of solute atoms during eutectic phase shape changing process, the EPFAs finally form at the edge of eutectic grains and then contact with other grains.

3.2. The SHD behavior of Sc element in eutectic Al–Fe–Ni-xSc alloy

3.2.1. The phenomenon of SHD and its influence on microstructure

Fig. 2a exhibits a typical microstructure of Al–Fe–Ni-*x*Sc alloys, and the Al matrix is subdivided into three parts labeled as: (1) primary Al, (2) eutectic boundary Al (i.e., eutectic phase free area (EPFA)), and (3) eutectic internal Al. Fig. 2b exhibits EDS analyses on these areas. Firstly, the Sc concentration of each eutectic internal Al is around the nominal Sc addition, and always a little higher than primary Al. Furthermore, EPFA has the highest Sc concentration of about twice of the corresponding nominal Sc addition. This phenomenon is expected if the EPFA is deemed as a kind of GB since Sc tends to aggregate at GB in Al–Sc alloys [4,5]. Specifically, Sc distribution is quite uneven in eutectic alloys (Fig. 2b), and it is identified as the SHD phenomenon.

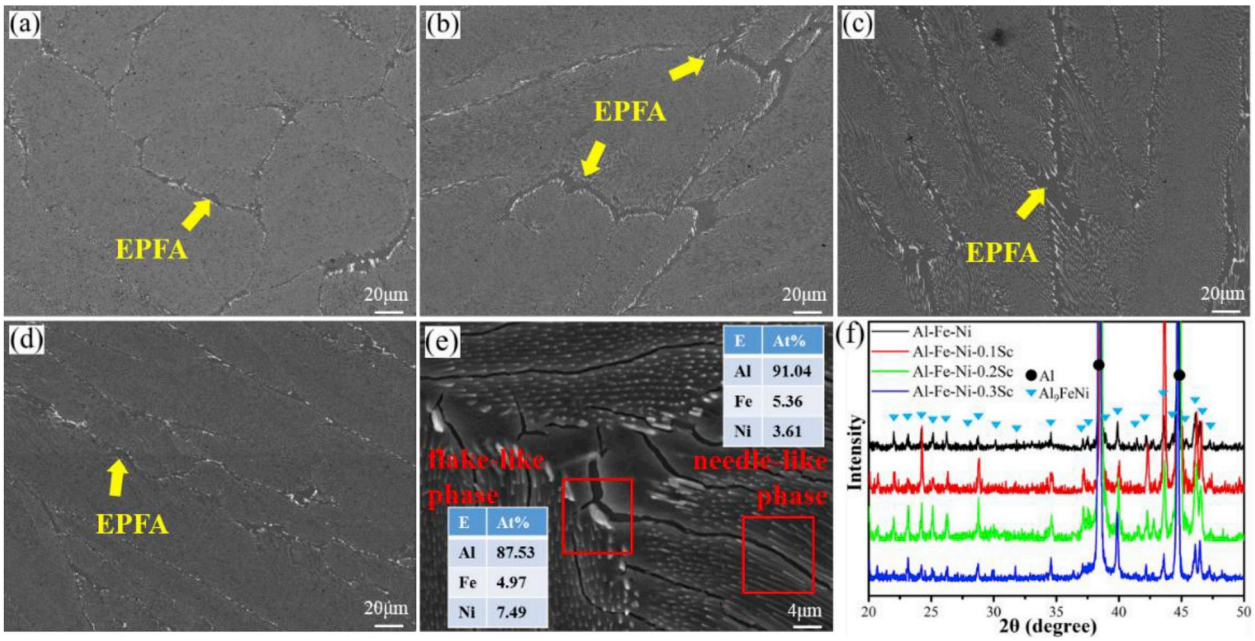

Fig. 1. As-cast microstructures of (a) Al–Fe–Ni alloy; (b) Al–Fe–Ni-0.1Sc alloy; (c) Al–Fe–Ni-0.2Sc alloy; (d) Al–Fe–Ni-0.3Sc alloy. (e) Local GB area in Al–Fe–Ni after deep-etched; (f) XRD patterns of each alloy.

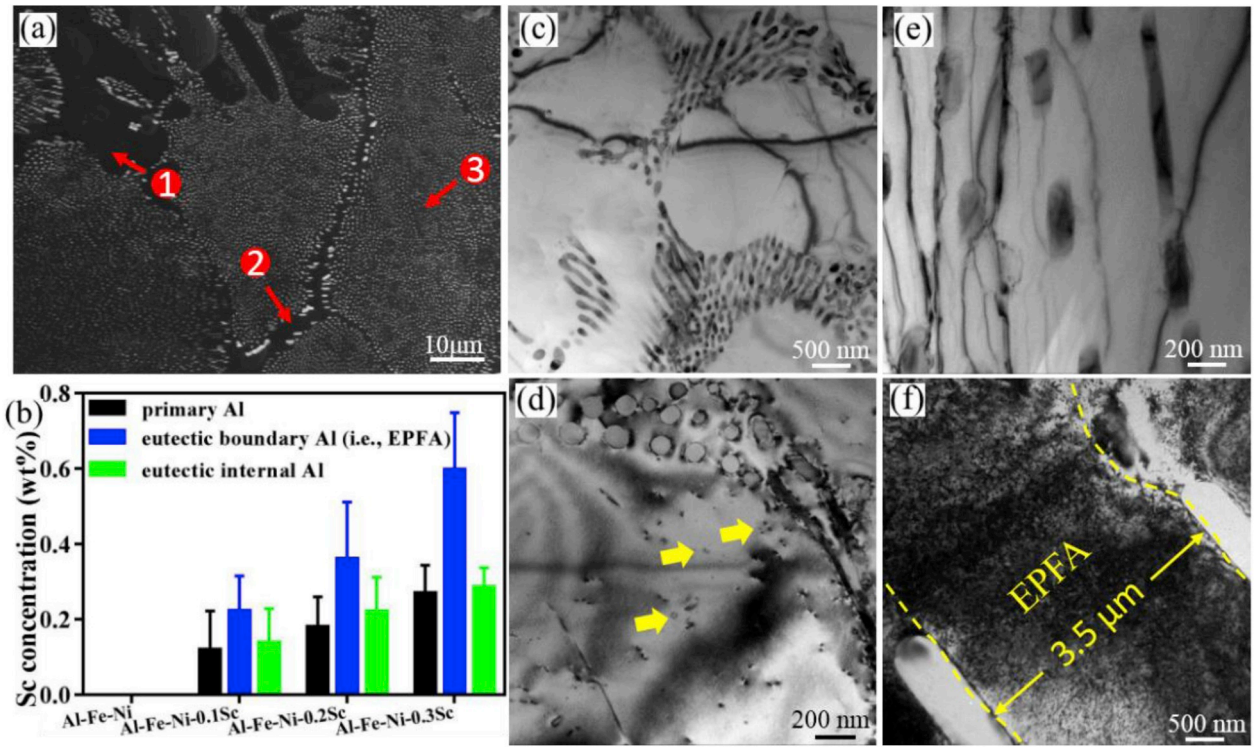

Fig. 2. (a) Three Al matrix sub-divisions of eutectic alloy; (b) Sc concentration in different subdivisions. Al_3Sc distribution in subdivisions of Al–Fe–Ni-0.2Sc alloy (Aged at 300 °C for 4 h): (c) interior of primary Al; (d) GB of primary Al; (e) eutectic internal Al; (f) EPFA.

Normally, the Sc distribution is reflected by precipitates distribution, if Al_3Sc precipitates are rarely influenced by Fe and/or Ni (Fig. 3). For example, Suwanpreecha et al. [25] reported that Ni hardly influenced Al_3Sc precipitates in Al–Ni-Sc alloys. In this work, the Sc distribution (Fig. 3d) shows that some round particles distribute randomly and their positions are in accordance with the positions of gray scale contrast in Fig. 3a. This correspondence gives the positions of precipitates. The corresponding distributions of Fe and Ni do not exhibit the possibility of other precipitates (Fig. 3b–c). The SAED pattern is exhibited in Fig. 3e, and the super-lattice suggests that the precipitates possess $L1_2$ structure. The high resolution transmission electron microscope (HRTEM) image of a specific particle is shown in Fig. 3f, and the Fast Fourier Transform of particle lattice is given as the insert. Therefore, an accurate super-lattice pattern can be observed to confirm that the precipitates are coherent with Al matrix. The image is taken from [011] axis, thus the interplanar spacing of (011) of Al_3Sc is measured from image directly.

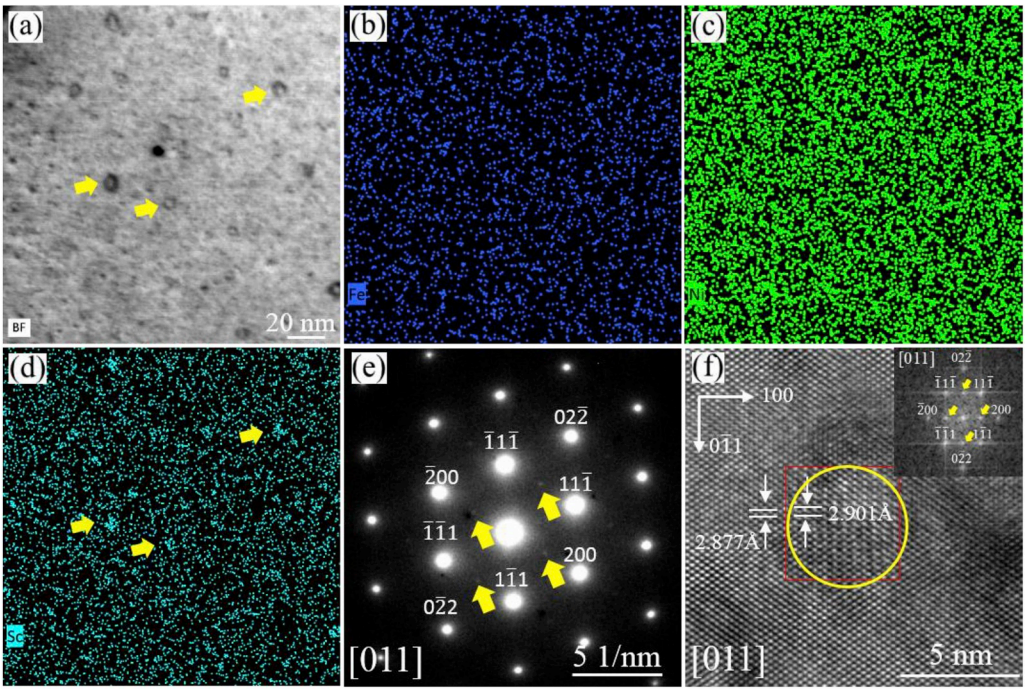

Fig. 3. (a) An EPFA with Al_3Sc precipitates of Al–Fe–Ni-0.2Sc alloy (Aged at 300 °C for 4 h); element distribution in this area:(b) Fe, (c) Ni, (d) Sc; (e) SAED pattern of this area; (f) HRTEM of a specific Al_3Sc particle.

This value can be identified as ~2.901 Å, which is the same as the reported value in literature [3]. In general, both Fe and Ni elements are found ever affected Al_3Sc precipitates in Al–Fe–Ni alloys.

Furthermore, the TEM micrographs of subdivisions in Al–Fe–Ni-0.2Sc alloy are shown in Fig. 2c–f. The alloy is annealed at 300 °C for 4 h, and all these images are taken under [011] axis. Al_3Sc precipitates present Ashby-Brown contrast at this condition since they are coherent with Al matrix [38]. The precipitates are more frequently observed near GB compared to the interior of primary Al (Fig. 2c–d, i.e., the arrows marked in Fig. 2d). In the eutectic internal Al, few Al_3Sc precipitates are observed apart from Al_9FeNi phase (Fig. 2e). Comparatively, a high density of precipitates is observed inside the EPFA (Fig. 2f). Evidently, Sc is surely to concentrate at EPFA, as corresponded to EDS results (Fig. 2b).

Subsequently, the morphologies of eutectic grains are shown in Fig. 4a–d, and the corresponding EBSD patterns are exhibited in Fig. 4e–h. It is noticed that most EPFAs symbolize the sub-grains boundary as the morphology features presented in SEM images and weak misorientation presented in EBSD patterns. Notably, tiny Al grains are locally induced in Al–Fe–Ni-0.3Sc alloy, and these grains are only found inside EPFAs. These grains are unexpected in the dilute Al–Sc alloys, though Sc is probably enriched at GBs [4,5,13]. Due to the SHD behavior, it is supposed that Sc concentration at EPFAs exceeds the eutectic composition in Al–Fe–Ni-0.3Sc alloy. Therefore, primary Al_3Sc should form inside EPFAs at the final stage of solidification to induce tiny grains.

3.2.2. *Theoretical prediction of SHD by a modified Scheil Equation*

Sc forms a terminal eutectic with Al, and the eutectic composition of Al–Sc system is ~0.6 wt% [1]. For Al–Fe–Ni-*x*Sc ($x = 0$, 0.1, 0.2, 0.3 wt %) alloys, the primary Al_3Sc is not supposed to form. During the eutectic solidification of Al–Al_9FeNi system, Sc also aggregates at the melt in front of solid [5], and finally forms a supersaturated solid solution with the higher concentration in EPFAs. Scheil Equation is used to estimate the Sc concentration in solid (C_s), supposing the negligible diffusion in the solid and complex mixing in the liquid [5]:

$$C_s = k_0 C_0 (1 - f_s)^{k_0 - 1} \quad (1)$$

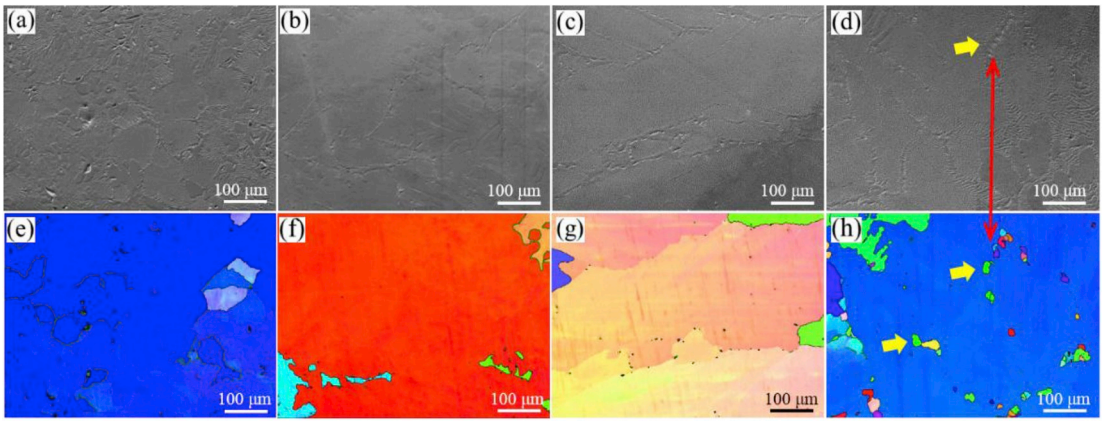

Fig. 4. As-cast SEM micrographs and EBSD patterns of (a), (d) Al–Fe–Ni; (b), (f) Al–Fe–Ni-0.1Sc; (c), (g) Al–Fe–Ni-0.2Sc; (d), (h) Al–Fe–Ni-0.3Sc.

where C_0 is the nominal Sc addition, and f_s is the fraction of the solidified part. The equilibrium solid-liquid partition coefficient k_0 is 0.8 [5], and the ideal situation between f_s and C_s is shown in Fig. 5a.

By integrating Equation (1), the relationship between the mean concentration of Sc at EPFAs (C_E), and the volume fraction of EPFAs calculated by Scheil Equation ($V_{E(theory)}$) can be obtained:

$$C_E V_{E(theory)} = C_0 V_{E(theory)}^{k_0} \tag{2}$$

Detected by EDS, C_E is about $2C_0$ (Fig. 2b). Substituting this value into Equation (2), $V_{E(theory)}$ is calculated as 3.1%, reflecting the maximum volume fraction of EPFAs, at which the mean Sc concentration satisfies $2C_0$. The schematic diagram for this theoretical situation is exhibited in Fig. 5b.

Through statistical analysis (i.e., Fig. 1a–d and Fig. 4a–d), the average diameter of the eutectic sub-grains (d_{eg}) is approximately 89.4 μm, and the average EPFAs width (d_{EPFAs}) is 3.7 μm. Thus, the practical volume fraction of EPFAs ($V_{E(test)}$) can be estimated by the experimental values via following equation:

$$V_{E(test)} = 1 - \left(\frac{d_{eg}/2}{d_{eg}/2 + d_{EPFAs}/2}\right)^3 \tag{3}$$

Thus, $V_{E(test)}$ is estimated as 11.5%, which is far larger than $V_{E(theory)}$. Therefore, this classical model may be inadequate to discuss Al–Fe–Ni-*x*Sc alloys and a modification is required to this model.

In the former research, it was convinced that Sc was seldom found in eutectic phase of Al–6Ni-0.2Sc and Al–6Ni-0.4Sc alloy [25]. Similar results can be found in the Al–Fe–Ni-*x*Sc alloy. For example, the element distribution around a eutectic phase in the Al–Fe–Ni-0.2Sc alloy is acquired in the scanning transmission electron microscopy (STEM) micrographs (Fig. 6). The detected region is around an Al_9FeNi eutectic phase (Fig. 6a). The element distributions of Al, Fe and Ni confirm that it is an Al_9FeNi eutectic phase. The Sc distribution illustrates that Sc barely aggregates inside the phase, and it mainly exists in Al matrix (Fig. 6d). In short, Sc is basically insoluble in Al_9FeNi, more Sc atoms are expected to be pushed from solid to the location where the solidification occurs lastly (i.e., the EPFAs).

In Al–Fe–Ni alloy, the mass fraction of Al_9FeNi is about 10.6 wt%, equaling to the volume fraction of 8.4 vol%. Then, the model can be modified in supposing that the eutectic structures solidify rapidly, in which Al_9FeNi cannot dissolve Sc and push all Sc into last solidified EPFAs:

$$C_E V_{E(theory)} = \left(C_0 - C_0 V_{E(theory)}^{k_0}\right) \times 8.4\% + C_0 V_{E(theory)}^{k_0} \tag{4}$$

The schematic diagram of the modified Scheil Equation is displayed in Fig. 5c. After substituting $2C_0$ into C_E of Equation (4), $V_{E(theory)}$ is calculated to be 13.3%. Generally, this theoretical result agrees well with the experiment value. Indeed, the SHD of Sc element exists in the eutectic alloy, arising from the influence of eutectic phases.

4. Discussion

In these Al–Fe–Ni-*x*Sc alloys, the SHD behavior of Sc element should induce a non-uniform strengthening effect on the alloy, which is different from what is previously deemed as a uniform Al_3Sc reinforcement [5]. Therefore, this non-uniform strengthening behavior may affect the strengthening efficiency of Sc addition, which should also be discussed hereafter.

4.1. The hardness test of Al–Fe–Ni-xSc in micro scale and macro scale

Table 2 exhibits the micro-hardness and the corresponding increments of three subdivisions in Al–Fe–Ni-*x*Sc tested by nano-indentation after annealing at 300 °C for 4 h. A local hardening behavior dependent on Sc distribution in the eutectic structure can be noted. Firstly, the EPFA shows the highest hardness especially in the Al–Fe–Ni-0.1Sc and Al–Fe–Ni-0.2Sc, and the eutectic internal area exhibits the highest hardness in Al–Fe–Ni alloy. Locally enriched by Sc, the intense local hardening strengthens EPFA more than other areas. Secondly, the hardness increment exhibits similar level where Sc possesses similar concentration. For instance, the Sc concentration in EPFA of Al–Fe–Ni-0.1Sc is close to that in primary Al and eutectic internal Al of Al–Fe–Ni-0.2Sc, and hardness increments in these areas are similar. Actually, the SHD behavior makes the Sc concentration in EPFA far higher than the nominal addition, causing that the local hardness increment reaches the level of that from higher nominal addition.

However, the hardness shows a reverse again when it comes to Al–Fe–Ni-0.3Sc as the eutectic internal area presents the highest hardness once again. This abnormal reverse results from the surprisingly lower increment observed in the EPFA of Al–Fe–Ni-0.3Sc, though the concentration of Sc in this area is the highest. This reduced increment is related to the microstructure evolution mentioned above. This abnormal reduction suggests that the excessive enrichment of Sc does not keep the solid solution state but promoting the formation of primary Al_3Sc phase. A sharp decrease is exhibited for the degree of supersaturation once Sc begins to form Al_3Sc primary phase, thus the hardness increment is affected and cut down.

Furthermore, the Vickers hardness test was performed on Al–Fe–Ni-*x*Sc to show the macro-hardness evolution. For example, the dependences of Vickers hardness (*HV*) variations on the aging durations at different temperatures of Al–Fe–Ni-0.2Sc alloy are exhibited in Fig. 7a. All samples were heat treated directly after casting. A three-stage aging process is seen at 275 °C,including incubation, precipitation and peak-age stages. When the aging temperature increases, the *HV* curve (i.e. 350 °C) turns to another three stages gradually, where the incubation stage disappears, and the overage stage appears. Generally, these aging processes are similar to Al–Sc alloys [5,13,15], indicating that the strengthening from Al_3Sc precipitates in Al–Fe–Ni-*x*Sc alloys are rarely affected by the eutectic structure on a macro scale.

Since these eutectic alloys are designed for HT application, the precipitate stability is noteworthy. Clearly, the Al–Fe–Ni-*x*Sc alloys can

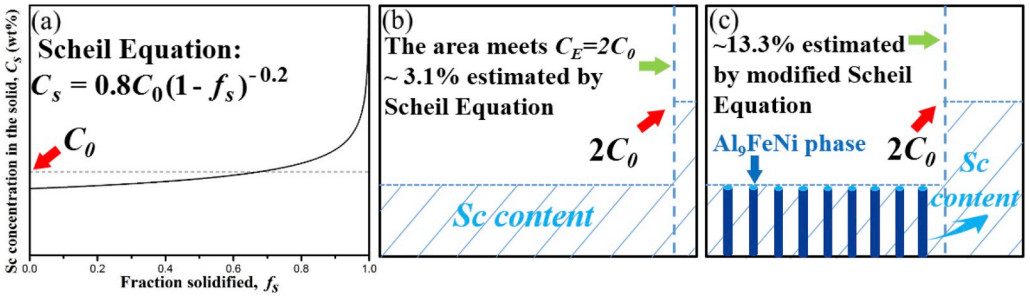

Fig. 5. (a) As-cast solute distribution calculated by Scheil model. (b) Schematic diagram of the maximum volume fraction of areas estimated by classic Scheil model. (c) Stimulated by Al_9FeNi phase, more Sc is pushed into final solidified EPFA area. A Modified Scheil Equation is applied to estimate this distribution.

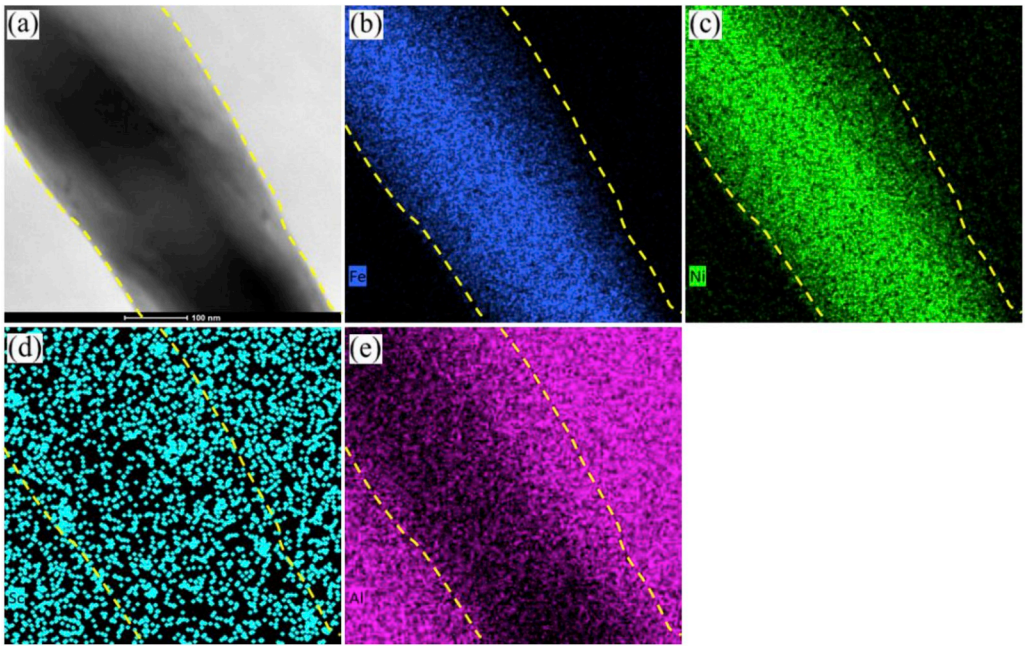

Fig. 6. Morphology of a Al_9FeNi phase in Al–Fe–Ni-0.2Sc alloy (Aged at 300 °C for 4 h) and the element distributions nearby:(a) part of Al_9FeNi phase in TEM; (b) Fe; (c) Ni; (d) Sc; (e) Al.

Table 2
Average micro-hardness values of three subdivisions for each alloy (Aged at 300 °C for 4 h) and the increment after adding Sc (MPa).

	Al–Fe–Ni	Al–Fe–Ni-0.1Sc	Δ	Al–Fe–Ni-0.2Sc	Δ	Al–Fe–Ni-0.3Sc	Δ
Primary Al	529.1 ± 14.8	707.1 ± 73.7	***178.6***	916.8 ± 82.0	***387.7***	1148.6 ± 48.1	***619.5***
EPFA	672.1 ± 101.6	1031.5 ± 20.2	***359.4***	1250.7 ± 20.4	***578.6***	1120.8 ± 32.1	***448.7***
Eutectic internal Al	718.9 ± 14.9	764.4 ± 23.8	***45.5***	1053.4 ± 92.7	***334.5***	1426.2 ± 62.8	***707.3***

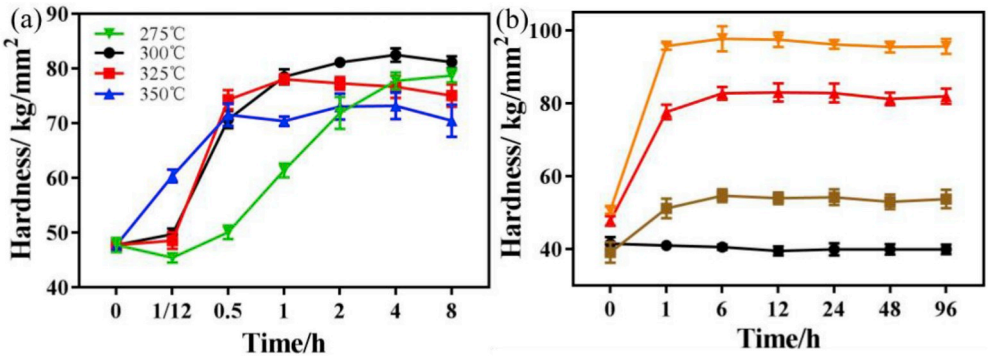

Fig. 7. Dependences of macro-hardness variations on the aging durations of (a) Al–Fe–Ni-0.2Sc alloy at different temperature; (b) Al–Fe–Ni-*x*Sc ($x = 0$, 0.1, 0.2, 0.3 wt%) alloys heat treated at 300 °C.

keep stable for at least 96 h at 300 °C (Fig. 7b). These stability is consistent with the Al_3Sc stability reported in literatures [13,15], which means the SHD behavior in eutectic structure and the structure itself should rarely influence the heat resistance of Al_3Sc.Above all, the Sc element can cause the hetereogeneous strengthening locally, while exhibiting the homogeneous hardening on a macro scale in eutectic alloys.

4.2. The correlation between micro-hardness and macro-hardness and the strengthening efficiency of Sc addition

The strengthening efficiency of Sc is reflected by the hardness increment. The relationship between macro-hardness increment (MAHI) and micro-hardness increment (MIHI) can be described:

$$H \bullet g = \sum_{i}^{n} h_i v_i \tag{5}$$

where H is the theoretical MAHI connected to MIHI;

g is a constant of 9.8 m/s^2 [39];
h_i and v_i are the MIHI and volume fraction of i_{th} part.

For simplicity, the eutectic alloy is considered as two parts. The first part is the Sc rich areas (i.e., EPFAs), and its volume fraction is ~11.5%. The MIHI of the EPFA is shown in Table 2. The second part is the Sc poor

areas including eutectic internal Al and primary Al, and its MIHI is adopted as the average value tested from both subdivisions. Thus, the theoretical MAHI connected to MIHI can be calculated as 14.3, 39.4 and 65.2 kg/mm^2, correspondingly. The experimental MAHI is 14.5, 43 and 55.8 kg/mm^2, accordingly (Fig. 7b). Therefore, a good consistency between the hardness enhancement level of micro test and macro test can be reached. Seidman et al. [13] reported the hardness increments for 0.1–0.3 wt% Sc addition in Al-*x*Sc alloy as 14.8, 44.9 and 56.1 kg/mm^2, accordingly. Based on our analyses and literature reports, the strengthening efficiency can be calculated as 98.0%, 95.8% and 99.5%, accordingly.

In addition, it is necessary to estimate the strengthening efficiency of Sc element in Al–Fe–Ni-*x*Sc alloys compared to that in Al–Sc alloy theoretically. In order to describe its contribution quantitatively, Sc is assumed to evenly distribute in Sc rich areas and Sc poor areas. Thus, the distribution of Sc in eutectic microstructure can be described as:

$$C_0 = C_0\eta_1 v_1 + \frac{C_0 - C_0\eta_1 v_1}{1 - v_1}(1 - v_1) \tag{7}$$

where C_0 is the nominal addition of Sc to the whole eutectic alloy; η_1 is the partition coefficient of Sc in the Sc poor areas; v_1 is the volume fraction of Sc poor areas.

Taendl et al. [40] found the average size of Al_3Sc precipitates mainly depended on the heat treatment temperature, while it barely has connection with the Sc concentration. Based on this point, it is assumed that the average sizes of Al_3Sc precipitates in different regions are the same. Thus, the enhancement from the Al_3Sc precipitates is just dependent on its volume fraction. Since the volume fraction of Al_3Sc precipitate is linear to the supersaturation of Sc, the hardness enhancement (Δ) can be described as:

$$\Delta = A\sqrt{C} \tag{8}$$

where A is a constant.

In combination with Equation (7), the strengthening of Sc in eutectic alloy can be described as average of each part:

$$\Delta = \Delta_{v_1} + \Delta_{v_2} = A\sqrt{C_0\eta_1}v_1 + A\sqrt{\frac{C_0 - C_0\eta_1 v_1}{1 - v_1}}(1 - v_1) \tag{9}$$

According to this formula, when the v_1 is a constant, with the range of η_1 from 0 to 1, the hardness improvement is reduced with the decrease of η_1. This means the heterogeneous Sc distribution should lower the strengthening efficiency to some extent. Under common cast condition, it is inevitable for Sc to distribute unevenly, and the Al_9FeNi phase aggravates the segregation of Sc in eutectic microstructure. Therefore, the strengthening efficiency of Sc in eutectic alloy may be further weakened.

According to experiment results, the volume fraction of EPFA in these eutectic alloys is estimated as 11.5 vol% during calculation, and the concentration of Sc in EPFA is about the twice of nominal addition. Under this condition, the distribution of Sc can be described as:

$$C_0 = 0.87 \times C_0 \times 0.885 + 2 \times C_0 \times 0.115 \tag{10}$$

Then, the strengthening efficiency of Sc can be estimated as:

$$\lambda = \frac{\sqrt{0.87C_0} \times 0.885 + \sqrt{2C_0} \times 0.115}{\sqrt{C_0}} = 0.988 \tag{11}$$

Equation (11) illustrates that though Sc distributes unevenly in the eutectic alloy, the strengthening efficiency of Sc do not reduce significantly. In this work, the experimental strengthening efficiencies of Al–Fe–Ni-*x*Sc ($x = 0$, 0.1, 0.2, 0.3 wt%) alloys are calculated as 98.0%, 95.8% and 99.5%, accordingly. It is noticed that the strengthening efficiency of 0.1 wt% Sc addition is basically coincident with theoretical prediction. When the addition of Sc is 0.2 wt%, the strengthening efficiency is lower than the prediction. It is speculated that this decrease arises from no homogenization treated to the sample. Since the samples were cooled in air during cast, they all experienced a long cooling period from HT, and some Al_3Sc may precipitate during this process. These precipitates are relatively large and reduce the strengthening efficiency of Sc. However, when the Sc addition reaches 0.3 wt%, the strengthening efficiency of Sc on the macro scale do not reduced as expected from micro-hardness variation. It is deduced that though the Sc enriches in local area and presents locally deteriorated strengthening efficiency, and it can induce intense refinement of grain or eutectic phase and promote extra strengthening so as to offset local strengthening efficiency loss. Generally, the SHD behavior of Sc element and corresponding local hardening rarely do harm to the strengthening efficiency of Al_3Sc in Al alloy.

5. Conclusion

In summary, this work demonstrates the SHD behavior of Sc element and the correlated local hardening behavior in the Al–Fe–Ni-Sc alloys. In combination the microstructure characterizations, hardness tests and theoretical analyses, the cause and influence of SHD can be summarized as follows:

(1) Owing to insolubility in Al_9FeNi, Sc is promoted to distribute further unevenly in this eutectic alloy, causing that the Sc concentration in EPFAs reaches about twice of the nominal addition.
(2) Analytically, this SHD behavior of Sc element can be described using a modified Scheil Equation by proposing that all the insoluble Sc are pushed into last solidified EPFAs.
(3) Corresponding to the Sc distribution, Al_3Sc aggregates mostly at the EPFAs, leading to the local hardening. Nevertheless, adding Sc can effectively induce the strengthening effect on the eutectic Al–Fe–Ni alloy at macro scale quantitatively.

Data availability

The raw/processed data required to reproduce these findings cannot be shared at this time as the data also forms part of an ongoing study.

Declaration of competing interest

On behalf of all authors, we declare that we have no financial and personal relationships with other people or organizations that can inappropriately influence our work, there is no professional or other personal interest of any nature or kind in any product, service and/or company that could be construed as influencing the position presented in, or the review of, the manuscript entitled, “Stimulated heterogeneous distribution of Sc element and its correlated local hardening effect in Al–Fe–Ni-Sc alloy”.

Acknowledgements

This work is sponsored by the National Key Research and Development Program of China (Grant No. 2018YFB1106302), Research Fund (Project No. 15X100040018) at Shanghai Jiao Tong University (China), and the project (Grant No. 2017WAMC002) sponsored by Anhui Province Engineering Research Center of Aluminum Matrix Composites (China).

References

[1] V.G. Davydov, T.D. Rostova, V.V. Zakharov, Y.A. Filatov, V.I. Yelagin, Scientific principles of making an alloying addition of scandium to aluminium alloys, Mater. Sci. Eng. A 280 (1) (2000) 30–36.
[2] G.M. Novotny, A.J. Ardell, Precipitation of Al_3Sc in binary Al-Sc alloys, Mater. Sci. Eng. A 318 (1–2) (2001) 144–154.
[3] J. Røyset, N. Ryum, Scandium in aluminium alloys, Int. Mater. Rev. 50 (1) (2005) 19–44.

[4] K.E. Knipling, R.A. Karnesky, C.P. Lee, D.C. Dunand, D.N. Seidman, Precipitation evolution in Al-0.1Sc, Al-0.1Zr and Al-0.1Sc-0.1Zr (at. %) alloys during isochronal aging, Acta Mater. 58 (15) (2010) 5184–5195.
[5] K.E. Knipling, D.C. Dunand, D.N. Seidman, Ambient- and high-temperature mechanical properties of isochronally aged Al-0.06Sc, Al-0.06Zr and Al-0.06Sc -0.06Zr (at. %) alloys, Acta Mater. 59 (3) (2011) 943–954.
[6] Y.H. Gao, J. Kuang, G. Liu, J. Sun, Effect of minor Sc and Fe co-addition on the microstructure and mechanical properties of Al-Cu alloys during homogenization treatment, Mater. Sci. Eng. A 746 (2019) 11–26.
[7] Y.C. Ye, L.J. He, P.J. Li, Differences of grain-refining effect of Sc and Ti additions in aluminum by empirical electron theory analysis, Trans. Nonferrous Metals Soc. China 20 (3) (2010) 465–470.
[8] T.G. Nieh, L.M. Hsiung, J. Wadsworth, R. Kaibyshev, High strain rate superplasticity in a continuously recrystallized Al-6%Mg-0.3%Sc alloy, Acta Mater. 46 (8) (1998) 2789–2800.
[9] A.B. Spierings, K. Dawson, P.J. Uggowitzer, K. Wegener, Influence of SLM scan-speed on microstructure, precipitation of Al_3Sc particles and mechanical properties in Sc- and Zr-modified Al-Mg alloys, Mater. Des. 140 (2018) 134–143.
[10] G. Li, N.Q. Zhao, T. Liu, J.J. Li, C.N. He, C.S. Shi, E.Z. Liu, J.W. Sha, Effect of Sc/Zr ratio on the microstructure and mechanical properties of new type of Al-Zn-Mg-Sc-Zr alloys, Mater. Sci. Eng. A 617 (2014) 219–227.
[11] Y. Deng, Z.M. Yin, Q.L. Pan, G.F. Xu, Y.L. Duan, Y.J. Wang, Nano-structure evolution of secondary $Al_3(Sc_{1-x}Zr_x)$ particles during superplastic deformation and their effects on deformation mechanism in Al-Zn-Mg alloys, J. Alloy. Comp. 695 (2017) 142–153.
[12] Eckhard Nembach, Particle Strengthening of Metals and Alloys, 1997.
[13] D.N. Seidman, E.A. Marquis, D.C. Dunand, Precipitation strengthening at ambient and elevated temperatures of heat-treatable Al(Sc) alloys, Acta Mater. 50 (2002) 4021–4035.
[14] C.B. Fuller, D.N. Seidman, D.C. Dunand, Creep properties of coarse-grained Al(Sc) alloys at 300°C, Scr. Mater. 40 (6) (1999) 691–696.
[15] C.B. Fuller, D.N. Seidman, D.C. Dunand, Mechanical properties of Al(Sc,Zr) alloys at ambient and elevated temperatures, Acta Mater. 51 (16) (2003) 4803–4814.
[16] Y.H. Gao, C. Yang, J.Y. Zhang, L.F. Cao, G. Liu, J. Sun, E. Ma, Stabilizing nanoprecipitates in Al-Cu alloys for creep resistance at 300°C, Mater. Res. Lett. 7 (1) (2019) 18–25.
[17] Y.H. Gao, L.F. Cao, C. Yang, J.Y. Zhang, G. Liu, J. Sun, Co-stabilization of θ'-Al_2Cu and Al_3Sc precipitates in Sc-microalloyed Al-Cu alloy with enhanced creep resistance, Mater, Today Nano 6 (2019) 100035.
[18] C. Yang, D. Shao, P. Zhang, Y.H. Gao, J.Y. Zhang, J. Kuang, K. Wu, G. Liu, J. Sun, The influence of Sc solute partitioning on ductile fracture of Sc-microalloyed Al-Cu alloys, Mater. Sci. Eng. A 717 (2018) 113–123.
[19] Y. Du, Y.A. Chang, B. Huang, W. Gong, Z. Jin, H. Xu, Z. Yuan, Y. Liu, Y. He, F. Y. Xie, Diffusion coefficients of some solutes in fcc and liquid Al: critical evaluation and correlation, Mater. Sci. Eng. A 363 (1–2) (2003) 140–151.
[20] B.L. Silva, A. Garcia, J.E. Spinelli, The effects of microstructure and intermetallic phases of directionally solidified Al-Fe alloys on microhardness, Mater. Lett. 89 (2012) 291–295.
[21] C. Suwanpreecha, P. Pandee, U. Patakham, C. Limmaneevichitr, New generation of eutectic Al-Ni casting alloys for elevated temperature services, Mater. Sci. Eng. A 709 (2018) 46–54.
[22] Z.Y. Bian, S.H. Dai, L. Wu, Z. Chen, M.L. Wang, D. Chen, H.W. Wang, Thermal stability of Al-Fe-Ni alloy at high temperatures, J. Mater. Res. Technol. 8 (3) (2019) 2538–2548.
[23] M.K. Premkumar, A. Lawley, M.J. Koczak, Mechanical behavior of powder metallurgy Al-Fe-Ni alloys, Mater. Sci. Eng. A 174 (1994) 127–139.
[24] A. Michalcová, D. Vojtech, J. Čízek, I. Procházka, J. Drahokoupil, P. Novák, Microstructure characterization of rapidly solidified Al-Fe-Cr-Ce alloy by positron annihilation spectroscopy, J. Alloy. Comp. 509 (2011) 3211–3218.
[25] C. Suwanpreecha, J. Perrin Toinin, R.A. Michi, P. Pandee, D.C. Dunand, C. Limmaneevichitr, Strengthening mechanisms in Al-Ni-Sc alloys containing Al_3Ni microfibers and Al_3Sc nanoprecipitates, Acta Mater. 164 (2019) 334–346.
[26] P. Pandey, S.K. Makineni, B. Gault, K. Chattopadhyay, On the origin of a remarkable increase in the strength and stability of an Al rich Al-Ni eutectic alloy by Zr addition, Acta Mater. 170 (2019) 205–217.
[27] R.A. Michi, J.P. Toinin, D.N. Seidman, D.C. Dunand, Ambient- and elevated-temperature strengthening by Al_3Zr Nanoprecipitates and Al_3Ni-Microfibers in a cast Al-2.9Ni-0.11Zr-0.02Si-0.005Er (at.%) alloy, Mater. Sci. Eng. A 759 (2019) 78–89.
[28] J.M. Kim, H.S. Yun, J.S. Shin, K.T. Kim, S.H. Ko, Mold filling ability and hot cracking susceptibility of Al-Fe-Ni alloys for high conductivity applications, J. Teknol. 75 (2015) 71–77.
[29] A. Leenaers, S.V.D. Berghe, E. Koonen, S. Dubois, M. Ripert, Post-irradiation examination of AlFeNi cladded U_3Si_2 fuel plates irradiated under severe conditions, J. Nucl. Mater. 375 (2008) 243–251.
[30] M. Wintergerst, N. Dacheux, F. Datcharry, E. Herms, B. Kapusta, Corrosion of the AlFeNi alloy used for the fuel cladding in the Jules Horowitz research reactor, J. Nucl. Mater. 393 (2009) 369–380.
[31] T. Koutsoukis, M.M. Makhlouf, An alternative eutectic system for casting aluminum alloys I. Casting ability and tensile properties, Light Met. (2015) 277–281.
[32] T. Koutsoukis, M.M. Makhlouf, Alternatives to the Al-Si eutectic system in aluminum casting alloys, Int. J. Metalcast. 10 (2016) 342–347.
[33] L. Zhang, J. Wang, Y. Du, R. Hu, P. Nash, X.G. Lu, C. Jiang, Thermodynamic properties of the Al-Fe-Ni system acquired via a hybrid approach combining calorimetry, first-principles and CALPHAD, Acta Mater. 57 (2009) 5324–5341.
[34] G.X. Hu, X. Cai, Y.H. Rong, Fundamentals of Materials Science, third ed., Shanghai Jiao Tong University Press, Shanghai, 2010.
[35] B. Chalmers, Principles of Solidification, John Wiley & Sons, New York, 1964, pp. 126–128.
[36] M.C. Flemings, Solidification Processing, McGraw-Hill, New York, 1974, pp. 31–32.
[37] W. Kurz, D.J. Fisher, Fundamentals of Solidification, forth ed., Trans Tech Publications, Aedermannsdorf, 1998, p. 15.
[38] A. Tolley, V. Radmilovic, U. Dahmen, Segregation in $Al_3(Sc,Zr)$ precipitates in Al-Sc-Zr alloys, Scr. Mater. 52 (7) (2005) 621–625.
[39] A. Inoue, K. Ohtera, A.P. Tsai, T. Masumoto, Aluminum-based amorphous alloys with tensile strength above 980 MPa (100 kg/mm^2), Jpn. J. Appl. Phys. 27 (4) (1988) L479–L482.
[40] J. Taendl, A. Orthacker, H. Amenitsch, G. Kothleitner, C. Poletti, Influence of the degree of scandium supersaturation on the precipitation kinetics of rapidly solidified Al-Mg-Sc-Zr alloys, Acta Mater. 117 (2016) 43–50.